Mobility gap in fractional quantum Hall liquids: Effects of disorder and layer thickness

Xin Wan,[1,2] D. N. Sheng,[3] E. H. Rezayi,[4] Kun Yang,[5] R. N. Bhatt,[6] and F. D. M. Haldane[7]
[1]*Institut für Nanotechnologie, Forschungszentrum Karlsruhe, 76021 Karlsruhe, Germany*
[2]*Zhejiang Institute of Modern Physics, Zhejiang University, Hangzhou 310027, People's Republic of China*
[3]*Department of Physics and Astronomy, California State University, Northridge, California 91330, USA*
[4]*Physics Department California State University Los Angeles, Los Angeles, California 90032, USA*
[5]*National High Magnetic Field Laboratory and Department of Physics, Florida State University, Tallahasse, Florida 32306, USA*
[6]*Department of Electrical Engineering, Princeton University, Princeton, New Jersey 08544, USA*
[7]*Department of Physics, Jadwin Hall, Princeton University, Princeton, New Jersey 08544, USA*
(Received 23 May 2005; published 10 August 2005)

We study the behavior of two-dimensional electron gas in the fractional quantum Hall regime in the presence of finite layer thickness and correlated disordered potential. Generalizing the Chern number calculation to many-body systems, we determine the mobility gaps of fractional quantum Hall states based on the distribution of Chern numbers in a microscopic model. We find excellent agreement between experimentally measured activation gaps and our calculated mobility gaps, when combining the effects of both disordered potential and layer thickness. We clarify the difference between mobility gap and spectral gap of fractional quantum Hall states and explain the disorder-driven collapse of the gap and the subsequent transitions from the fractional quantum Hall states to the insulator.

DOI: 10.1103/PhysRevB.72.075325 PACS number(s): 73.43.Lp, 73.43.Nq, 73.43.Qt

I. INTRODUCTION

One of the most remarkable properties of two-dimensional electron gas (2DEG) is the amazing precision of the Hall resistivity quantization $\rho_{xy}=h/(ie^2)$ in a perpendicular high magnetic field at low temperatures, regardless of materials, geometries, impurities, and carrier concentrations of experimental systems. This phenomenon is known as the integer quantum Hall effect[1] (IQHE) for integer i, or as the fractional quantum Hall effect[2] (FQHE) for certain fractional values of i. At the Hall resistivity plateaus, the longitudinal resistivity ρ_{xx} vanishes at zero temperatures, but has an Arrehenius-type temperature T dependence,

$$\rho_{xx} \propto \exp(-\Delta/2k_BT), \tag{1}$$

where k_B is the Boltzmann's constant.[3–5] The thermally activated behavior suggests that there is an activation gap $\Delta/2$ in the excitation spectrum of each quantum Hall state. The gap has an origin of Landau level spacing in the IQHE,[6] and a more profound origin of electron-electron interaction in the FQHE;[7] in fact, the existence of the activation gap leads directly to the Hall resistivity quantization and the consequent incompressibility of the corresponding Hall liquid at low temperature.

Theoretically, Δ in the FQHE is expected to be the creation energy of a pair of free quasielectron and quasihole. In a pure system, this is the asymptotic value of the excitation spectrum in the large momentum limit, found to be as large as $0.1e^2/\epsilon l_B$,[8,9] where ϵ is the dielectric constant and $l_B=(\hbar c/eB)^{1/2}$ the magnetic length. However, experiments[3–5] found much smaller excitation gaps, presumably due to the reduction caused by the presence of disorder, the thickness of the 2DEG layer, and the mixing of Landau levels. Yoshioka[10] combined the effects of layer thickness[11] and Landau level mixing,[12] and obtained reasonable agreement with experimental results in high-mobility systems at large enough magnetic fields.[5]

However, without taking into account the effects of disorder, theoretical considerations cannot explain the vanishing activation energy below finite magnetic field (about 5 T).[4,5] Qualitatively, disorder broadens the quasielectron-quasihole excitation band, leading to a reduction of the energy gap between the ground state and excited states.[3] MacDonald *et al.*[13] and Gold[14,15] considered the effects of disorder. Both theoretical approaches contain adjustable parameters, and more importantly, fail to answer the following crucial questions: Which quasielectron-quasihole excitations are contributing to the activated longitudinal resistivity? What is the nature of the activation gap?

To answer these questions, let us look at the single-particle picture of the IQHE first. In a clean system with exactly n (labeled from 0 to $n-1$) Landau levels filled, the activation gap is obviously the Landau level spacing $\hbar\omega_c$, where $\omega_c=eB/m^*c$ is the cyclotron frequency. This involves the excitation of an electron in the $(n-1)$th Landau level to the nth Landau level, or equivalently, the excitation of a pair of electron in the nth Landau level and hole in the $(n-1)$th Landau level. In the presense of disorder, each Landau level is broadened into a Landau band (with bandwidth 2Γ, say). Due to Anderson localization, localized states exist in the tails of each band, and delocalized states only exist in the center of the band (where the mobility edge is). The excitation of an electron from a localized level to another does not contribute to the longitudinal resistivity; only excitations involving delocalized levels matter. Therefore although the spectral gap in this case is reduced to $(\hbar\omega_c-2\Gamma)$, the energy to excite a pair of free electron and free hole is still $\hbar\omega_c$—related to the mobility gap rather than the spectral gap of the system. In the FQHE, on the other hand, we have

quasielectron and quasihole excitations. Similar to electrons in the integer case, these quasiparticles can be trapped in their potential valleys and become localized, thus do not contribute to the longitudinal resistivity. Therefore we need to find, for the FQHE, the mobility edge—the energy beyond which quasiparticle excitations are delocalized.

In the noninteracting IQHE, the calculation of topologically invariant Chern numbers has been established[16–23] as a reliable way to obtain the Hall conductance, to measure the localization length critical exponent, and to determine whether a single-particle state is localized or conducting—thus where the mobility edge is. Physically, the Chern number of a state is the (dimensionless) Hall conductance, which can be derived from the Kubo formular, averaged over boundary conditions of a finite system on a torus.[17] In addition, it has an elegant geometric interpretation as the integral of the curvature of the quantum state in the parameter space spanned by two angular parameters (twisted boundary conditions)—the first Chern class of a U(1) principal fiber bundle on the torus.[24–26] Chern numbers are topologically invariant under small perturbations of Hamiltonian, such as weak disorder, which allows the mobility gap to open for a finite range of magnetic field, leading to the plateau structure of the IQHE as long as the Fermi level lies in the mobility gap.

However, the geometric interpretation of the Hall conductance leads to an apparent controversy[17,27] in the FQHE. On the one hand, if a system exhibits the FQHE, the many-body ground state of the system must be degenerate on a toroidal geometry; otherwise, gauge-invariance arguments produce only integral Hall conductance.[28] For a pure system at filling fraction $\nu=p/q$ (p and q relatively prime to each other), the ground-state manifold is q-fold degenerate. Generically, these q degenerate states share a total Chern number p, regardless of the Chern number carried by each state. Thus the Hall conductance of the pure system is the average Chern number of these q states, fractionally quantized at $\sigma_H = pe^2/qh$. However, numerical calculations show that impurities lift the degeneracy in a finite system,[29] implying that the Hall conductance would only be quantized to fractional values under superfluous conditions.[30]

Wen and Niu[31] proposed that states of a system exhibiting the FQHE are topologically degenerate on a torus (in general, on high-genus Riemann surfaces) in the thermodynamic limit. The ground-state degeneracy is, in fact, a signature of the topological order of the bulk, invariant against weak but otherwise arbitrary perturbations (including symmetry-breaking impurity potential).[32] In a finite system, the quasidegeneracy of the states replaces the exact degeneracy, which can be recovered in the thermodynamic limit. The topological degeneracy thus guarantees the Hall conductance to be quantized at fractional values in the fractional regime even in dirty systems, in which the topological Chern number for each many-body state is well defined. Based on these ideas, we performed a numerical study of topological Chern numbers for the $\nu=1/3$ FQHE in finite systems.[33] The mobility gap for the FQHE can be determined from the distribution of the Chern numbers of the quasidegenerate many-body states. The results quantitatively explain the absence of the activation gap of the FQHE due to disorder at small magnetic fields, as well as the disorder-driven collapse of the gap and the subsequent transition from the FQHE to insulator at higher fields, observed by various experiments.[3–5]

In this paper, we further apply the method of Chern number calculation to study the effects of layer thickness of 2DEG and correlated potential on mobility gaps of FQHE systems. In Sec. II, we introduce our microscopic model for 2DEG with disordered potential and finite layer thickness, and explain the Chern number calculation for FQHE systems. In Sec. III, we discuss the effects of layer thickness on the properties of 2DEG, in particular on mobility gaps, which we compare to the activation gaps measured by experiments. We then discuss the effects of correlated impurity potential on mobility gaps in Sec. IV before we summarize our results in Sec. V.

II. MODEL AND METHOD

We consider a two-dimensional (2D) polarized interacting electron system on an $L_1 \times L_2$ rectangular area with generalized periodic boundary conditions (PBCs)

$$T(\mathbf{L}_j)\Phi(\mathbf{r}) = e^{i\theta_j}\Phi(\mathbf{r}), \tag{2}$$

where $T(\mathbf{L}_j)$ is the magnetic translation operator and $j=1, 2$, representing x and y directions, respectively. In the presence of a strong magnetic field, one can project the Hamiltonian of the system onto the partially filled, lowest Landau level. Therefore we consider the following projected Hamiltonian in the presence of both Coulomb interaction and disorder:[33]

$$H = \frac{1}{A}\sum_{i<j}\sum_{\mathbf{q}} e^{-q^2/2}V(q)e^{i\mathbf{q}\cdot(\mathbf{R}_i-\mathbf{R}_j)} + \sum_i \sum_{\mathbf{q}} e^{-q^2/4}U_{\mathbf{q}}e^{i\mathbf{q}\cdot\mathbf{R}_i}, \tag{3}$$

where $\mathbf{R}_i$ is the guiding center coordinate of the ith electron, $U_{\mathbf{q}}$ is the impurity potential with wave vector $\mathbf{q}$, and

$$V(q) = \frac{2\pi e^2}{\epsilon q}F(q) \tag{4}$$

is the Fourier transform of the electron-elctron interaction. The factor $F(q)$ generalizes the Coulomb interaction to the case with finite electron layer thickness (to be explained in the next paragraph). We use the Gaussian white-noise potential generated according to the following correlation relation in q space:

$$\langle U_{\mathbf{q}}U_{\mathbf{q}'}\rangle = \frac{W^2}{A}\delta_{\mathbf{q},-\mathbf{q}'}, \tag{5}$$

which corresponds, in real space, to

$$\langle U(\mathbf{r})U(\mathbf{r}')\rangle = W^2\delta(\mathbf{r}-\mathbf{r}'), \tag{6}$$

where W is the strength of the disorder (in units of e^2/ϵ) and $A=2\pi N_s l_B^2$ is the area of the system. To study the effects of correlated potential, we also generate the Gaussian correlated random potential $U(r)$ according to

$$\langle U_{\mathbf{q}}U_{\mathbf{q}'}\rangle = \frac{W^2}{A}\delta_{\mathbf{q},-\mathbf{q}'}e^{-q^2\xi^2/2}, \tag{7}$$

which leads to

$$\langle U(\mathbf{r})U(\mathbf{r}')\rangle = \frac{W^2}{2\pi\xi^2} e^{-|\mathbf{r}-\mathbf{r}'|^2/2\xi^2}, \tag{8}$$

where ξ is the characteristic correlation length. Note that in the limit of $\xi \to 0$, we recover the Gaussian white-noise potential.

To describe the thickness of a quasi-two-dimensional electron system, we employ the Fang-Howard variational wave function

$$\phi(z) = (b^3/2)^{1/2} z e^{-bz/2}, \tag{9}$$

where b depends on the material properties and the carrier density of the system. The parameter b^{-1} has the physical meaning of electron layer thickness, thus we will use, unless otherwise specified, the dimensionless layer thickness $\beta = (bl_B)^{-1}$ hereafter. The experimentally interesting range of parameter is $\beta \sim 1$. For the Fang-Howard wave function, the reduced Coulomb interaction in two dimensions becomes[11]

$$V(r) = (e^2/\epsilon) \int_0^\infty dq F(q) J_0(qr), \tag{10}$$

where

$$F(q) = \left(1 + \frac{9}{8}\frac{q}{b} + \frac{3}{8}\frac{q^2}{b^2}\right)\left(1 + \frac{q}{b}\right)^{-3} \tag{11}$$

and J_0 is the Bessel function of zeroth order. This factor $F(q)$, the same as in Eq. (4), softens the bare Coulomb interaction between electrons, especially at short distances.

We diagonalize the Hamiltonian with Lanczos algorithm and compute the Hall conductance σ_H through the Chern number calculation, which offers an unambiguous criterion to distinguish between insulating and current carrying states in an interacting system.[18,33] With a unitary transformation

$$\Psi_k = \exp\left[-i\sum_{i=1}^{N_e}\left(\frac{\theta_1}{L_1}x_i + \frac{\theta_2}{L_2}y_i\right)\right]\Phi_k, \tag{12}$$

we can write the boundary-condition averaged Hall conductance for the kth many-body eigenstate Φ_k as $\sigma_H(k) = C(k)e^2/h$, where the Chern number $C(k)$ for the state is

$$C(k) = \frac{i}{4\pi}\oint_\Gamma d\theta\left[\left\langle\Psi_k\middle|\frac{\partial\Psi_k}{\partial\theta}\right\rangle - \left\langle\frac{\partial\Psi_k}{\partial\theta}\middle|\Psi_k\right\rangle\right]. \tag{13}$$

Here, the closed path integral is carried out along the boundary Γ of the boundary condition space (the magnetic Brillouin zone) $0 \leqslant \theta_1, \theta_2 \leqslant 2\pi$. $C(k)$ is exactly the Berry phase (in units of 2π) accumulated for the state when the boundary conditions evolve along Γ. We separate the magnetic Brillouin zone into at least 25 meshes depending on the system size and calculate the sum of the Berry phase from each mesh. For the mesh sizes we choose, we find converged integer Chern numbers. We emphasize that throughout the paper we use the rectangular geometry, which facilitates the calculation of Chern numbers. A heuristic but qualitative discussion on the ground-state splitting and localized quasiparticle excitations also exists for a spherical geomotry.[34]

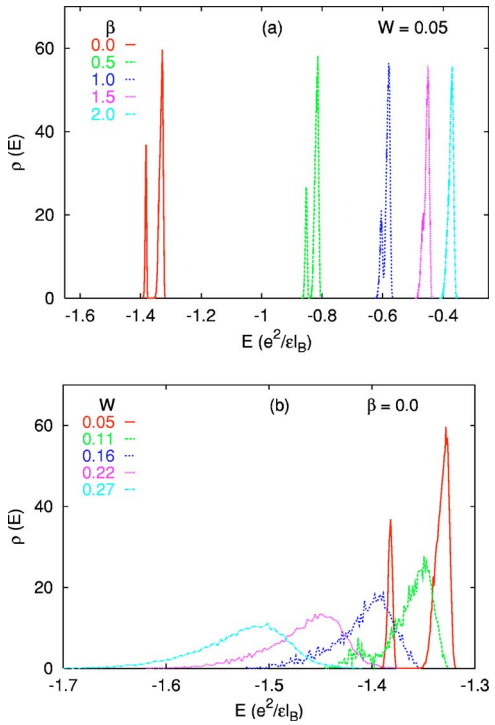

FIG. 1. (Color online) Density of the lowest 15 many-body states for $N_e=6$ at $\nu=1/3$. (a) $W=0.05$ with $\beta=0.0$, 0.5, 1.0, 1.5, and 2.0. (b) $\beta=0.0$ with $W=0.05$, 0.11, 0.16, 0.22, and 0.27.

III. EFFECTS OF LAYER THICKNESS

In this section, we discuss the effects due to the finite thickness of the 2DEG for $\nu=1/3$. We use the Fang-Howard variational wave function, introduced in Sec. II, to describe the electronic wave function in the perpendicular direction. We consider the Gaussian white-noise potential, and compare the disorder effects to the ideal two-dimensional case.[33] In the following subsections, we present results on density of state, energy, and energy split of ground states, spectral gap, distribution of Chern numbers, and mobility gap. These results are qualitatively similar for cases with and without finite layer thickness.

A. Density of states

We diagonalize the system to obtain up to 30 lowest states for each sample for $N_e=3$–8. Figure 1(a) shows the evolution of the many-body density of the 15 states as the layer thickness changes in the upper panel for weak disorder $W=0.05$ and system size $N_e=6$. For $W=0.05$ and $\beta=0.0$, a spectral gap is visible in the density of states with the low-energy peak consisting of three nearly degenerate states. As β increases, the energies of states becomes closer to zero while the spectral gap narrows, reflecting the softening of the Coulomb interaction. For $\beta=2.0$, even a weak $W=0.05$ is sufficient to destroy the spectral gap completely. For comparison, Fig. 1(b) shows the evolution of the density of the 15 states as W increases for zero layer thickness $\beta=0.0$ in the lower panel. Disorder broadens the density of states and the low-energy peak merges with other states at $W>0.11$ for $N_e=6$.

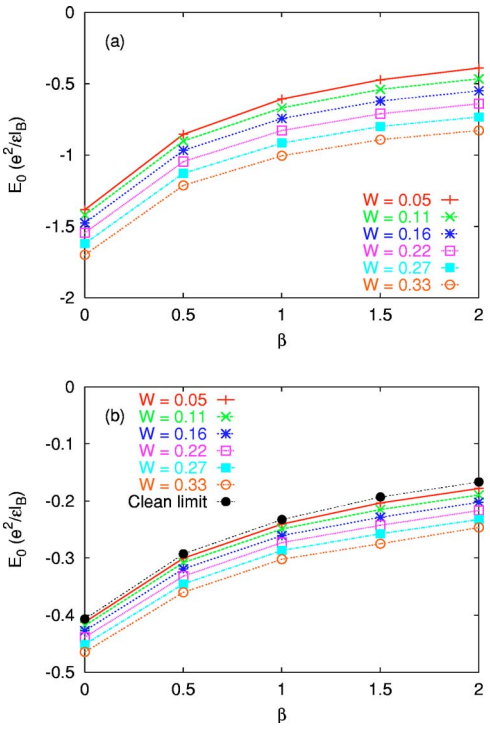

FIG. 2. (Color online) (a) Ground-state energy (excluding interaction between electrons and their images) as a function of β for $N_e=6$ at $\nu=1/3$. (b) Ground-state energy per electron, extrapolated to the thermodynamic limit, as a function of β for $\nu=1/3$.

B. Ground-state energy

The effects of the finite layer thickness on the ground-state energy of the fractional quantum Hall effect has been considered by MacDonald and Aers.[35] In the absense of disorder, they found that the the Laughlin state energy at $\nu=1/3$ for $\beta=1.0$ reduces to 0.576 of its value for $\beta=0.0$. Chakraborty[36] found a similar reduction ratio of 0.579 using the hypernetted-chain method.

In the presence of disorder, we find a similar reduction in magnitude of the many-body ground-state energy E_0 in finite systems. Figure 2(a) shows the reduction of the ground-state energy as a function of β for $N_e=6$ at $\nu=1/3$. Here, we defined the ground-state energy as the average energy of the lowest three levels, which are topologically degenerate in the thermodynamic limit. To compare our results with earlier works,[35,36] we first add, to the many-body ground-state energy, a single-particle contribution from interactions of an electron and its images due to periodic boundary conditions. This energy can be related to the Coulomb energy of the classical square Wigner crystal with finite layer thickness.[45] We then extrapolate our data for $N_e=3$–7 electrons to the thermodynamic limit according to

$$E_0(N_e) = E_0(N_e \to \infty) + a_0/N_e. \tag{14}$$

The results for ground-state energy per electron are shown in Fig. 2(b). By extrapolating the results to the clean limit by a quadratic fit, we obtain a reduction ratio of 0.572 for the ground-state energy from $\beta=0.0$ to $\beta=1.0$. The value is in good agreement with known results in the clean case.[35,36] In the presence of the impurity potential, disorder shifts the ground-energy state down, leading to a slightly larger ratio (e.g., 0.596 for $W=0.11$).

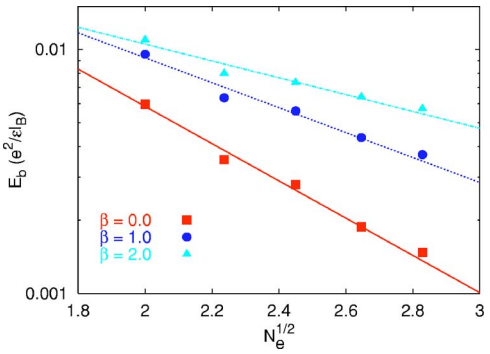

FIG. 3. (Color online) Energy split of ground states as a function of the square root of electron number (linear system size) on a semilog scale for various β at $W=0.05$ and $\nu=1/3$.

In the current and earlier works,[35,36] the ground-state energy is negative, due to the assumption of a uniform neutralizing background charge, which cancels out the singular contribution of the Coulomb interaction among electrons. Mathematically, we substract the singular $q=0$ contribution from the electron-electron interaction, as illustrated in Appendix A. Therefore a reduction of E_0 in magnitude is, in fact, an increase of the ground-state energy, as layer thickness increases. This is mainly because the corresponding reduction of the attractive interaction between electrons and the background charge negates the contribution from the softening of the electron-electron repulsion. Meanwhile, E_0 decreases with increasing W because electrons take advantage of the negative potential region in the ground state as shown in Fig. 2.

C. Energy split of the ground states of finite systems

Wen and Niu[31] pointed out that the ground states of the fractional quantum Hall state are degenerate on a torus even in the presence of disorder. However, this is strictly valid only in the thermodynamic limit. For a finite system on a torus of length L, the ground states have an energy split, or a bandwidth E_b, of order

$$E_b \sim e^{-L(m^*\Delta)^{1/2}}, \tag{15}$$

where Δ is the quasiparticle-quasihole pair creation energy and m^* is the effective mass of the quasiparticle. The energy split comes from the tunneling process that a virtually created pair of quasiparticle and quasihole propagate in opposite directions and annihilate on the other side of the torus.

In Fig. 3, we plot the bandwidth E_b of the lowest three states, which are well separated from all higher levels at $\nu=1/3$ and $W=0.05$, as a function of $\sqrt{N_e}$, proportional to the linear system size. For various β, the decrease of E_b with $\sqrt{N_e} \sim L$ is consistent with the exponential decrease in Eq. (15) expected by the theory,[31] as found in Ref. 33 for zero layer thickness, though we cannot completely rule out a power-law decrease of E_b based on these finite-size values. We find E_b increases with the layer thickness, again consis-

tent with Eq. (15) assuming that the quasiparticle-quasihole pair creation energy decreases with increasing β, as the Coulomb repulsion between electrons reduces. From $\beta=0.0$–1.0, the slope in the semilog plot of Fig. 3 reduces by roughly 30%. The reduction is, however, smaller than that of either the spectral gap or the mobility gap which we will discuss in the following sections.

We also note that a weak periodic potential, instead of disorder, gives rise to a similar exponential dependence of the splitting on system size,[37] implying, again, a degenerate ground-state manifold in the thermodynamic limit. The nontrivial ground-state degeneracy, existing on Riemann surfaces with genus 1 (torus) or greater,[31] is a signature of topological order[32] possessed by these states. The basic physics of the topological degeneracy and the finite-size splitting of the ground-state manifold in FQHE is the same as in chiral spin liquid, which is also a prototype for studying topological order and quantum error-correcting code.[38]

D. Spectral gap

Since the ground-state manifold on a torus consists of three quasidegenerate levels for $\nu=1/3$, we define the spectral gap as the energy difference between the third and the fourth lowest energy states

$$E_s = E(4) - E(3). \tag{16}$$

At large disorder, E_s simply becomes the energy level spacing, when the lowest three levels no longer form a separate band from higher levels.

We extrapolate E_s to the thermodynamic limit by fitting E_s to

$$E_s(N_e) = E_s(N_e \to \infty) + a_s/N_e. \tag{17}$$

Figure 4(a) shows $E_s(N_e \to \infty)$ as a function of β for various W at $\nu=1/3$. For small W, E_s decreases as β increases, or as the electron layer becomes thicker. For large W, E_s remains smaller than or close to 0.003, reflecting the closure of the spectral gap of the quantum Hall liquid. This finite but small residual value comes from the energy-level spacing of the insulating phase, which may disappear with a more sophisticate definition of the spectral gap. In fact, for fixed layer thickness, E_s first decreases with increasing disorder, then increases weakly with disorder after reaching its minimum. This minimum signals the critical disorder at which the spectral gap closes in the thermodynamic limit.

E. Groups of Chern numbers and their statistics

Due to the topological threefold degeneracy of the each energy level in the thermodynamic limit for $\nu=1/3$ quantum Hall liquids on a torus, we define the N_gth group of states as the $(3N_g-2)$th, $(3N_g-1)$th, and $(3N_g)$th states, and calculate the Chern number of such a group $C(N_g)$ as the sum of the Chern numbers of the three states within the group. While for small enough disorder, the states within each group are degenerate in the thermodynamic limit, this no longer holds for disorder strength large enough to distroy the fractional quantum Hall phase and the accompanying topological order.

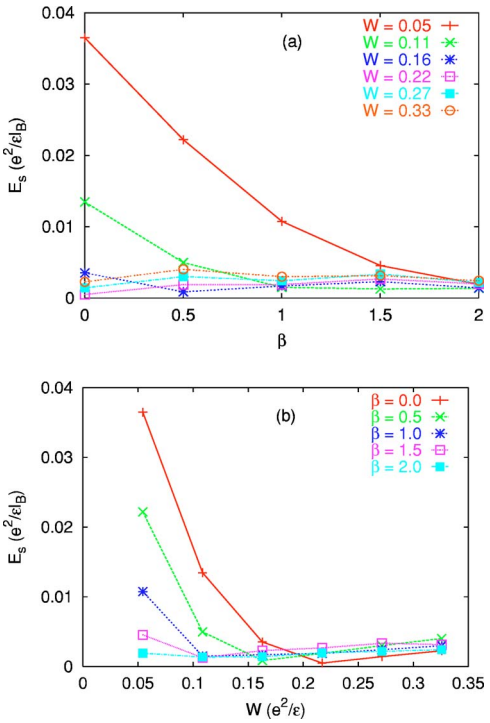

FIG. 4. (Color online) Spectral gap, extrapolated to the thermodynamic limit, (a) as a function of β for various W, and (b) as a function of W for various β at $\nu=1/3$.

In earliar work,[33] we found the following properties for the statistics of the group Chern numbers for two-dimensional electrons at $\nu=1/3$ with zero layer thickness.

(i) For weak disorder, the Chern number of the lowest group is always unity, carried by the three lowest states. This together with the fact that the three states become degenerate in the thermodynamic limit, as well as the fact that there is a finite spectral gap separating the three states to the rest, is the manifestation of the $\nu=1/3$ fractional quantum Hall state on a torus. In the thermodynamic limit, each degenerate ground state carries a Hall conductance of $e^2/3h$. This also holds for the Chern numbers of upper groups for small enough disorder.

(ii) Large enough disorder destroys the quantization of the Chern number of each group in individual samples from upper groups down to the lowest one. For certain disorder, the probability of the group Chern number being unity decreases sharply around one group, the energy of which we can define as the mobility edge. We will discuss the procedure in greater detail later in Sec. III F.

(iii) The Chern number calculation is robust for small systems with as few as five electrons. The fluctuation of the group Chern number has little size dependence, which therefore can be used as an robust indicator of the degree of delocalization.

Figure 2 in Ref. 33 summarizes these properties, which can be used to determine the mobility gap. We repeat the calculation in the presence of finite layer thickness. Figure 5 shows, in analog to Fig. 2 in Ref. 33, the probability distribution $P(C)$ for group Chern number C of the lowest five groups of states in systems of five to seven electrons for W

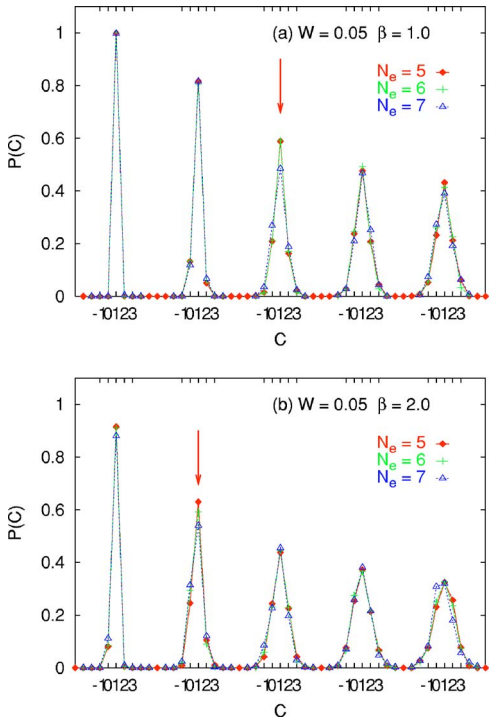

FIG. 5. (Color online) Probability distribution $P(C)$ of total Chern number C for the lowest five groups of states in systems of five to seven electrons for $W=0.05$ and for $\beta=1.0$ and 2.0. Energy increases from left to right. The arrow in each panel marks the group of states located at the mobility edge.

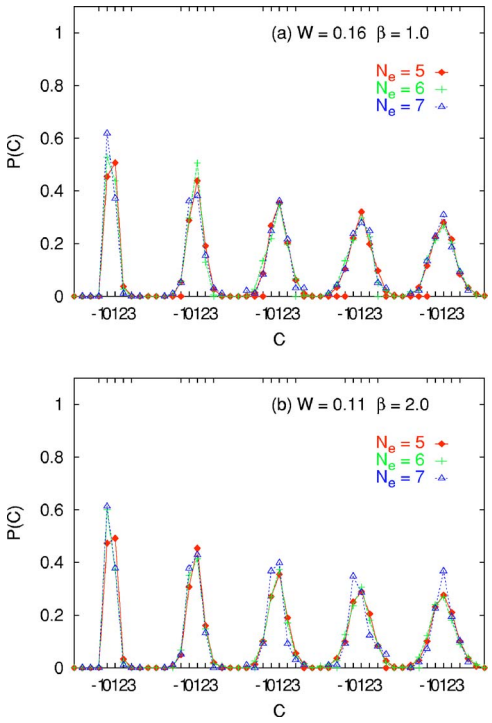

FIG. 6. (Color online) Probability distribution $P(C)$ of total Chern number C for the lowest five groups of states in systems of five to seven electrons for $W=0.16$ and 0.11 for $\beta=1.0$ and 2.0, respectively. Energy increases from left to right.

$=0.05$ and for $\beta=1.0$ and 2.0. We find that the above-mentioned properties remain intact qualitatively in the presence of finite layer thickness. Quantitatively, the increasing layer thickness shifts the mobility edge toward the ground state. For example, for $\beta=2.0$, the probility $P(C=1)$ of the lowest group is close to unity, suggesting that fractional quantum Hall phase survives at $W=0.05$. Meanwhile, $P(C=1)$ of the second lowest group drops sharply to about 0.6, and may drop further lower for larger systems. This indicates the location of the mobility edge.

We compare, in Fig. 6, the distribution $P(C)$ for larger disorder $W=0.16$ and 0.11 for $\beta=1.0$ and 2.0, respectively, again for the lowest five groups in five- to seven-electron systems. For the strong disorder, even the quantization of the lowest group no longer holds, which becomes much smaller than 1, indicating an insulating ground state in the thermodynamic limit.

F. Mobility gap

As discussed above, the fluctuation of the total Chern numbers in each group of states is an indication of the degree of delocalization, which we can used to determine the mobility edge. Similar as in Ref. 33, we define $P_{\text{ext}}=1-P(C=1)$. The value of P_{ext} is the probability of the breakdown of the Hall-conductance quantization and thus a measure of the delocalization of the charge excitations. This is analogous to the noninteracting IQHE case, where particle excitations from localized states to delocalized states lead to fluctuation of the total Chern number, or Hall conductance.

For small disorder, P_{ext} remains close to 0 for groups of states beyond the ground-state manifold. This reflects that the mobility gap (which separates localized states from delocalized states) is different from the spectral gap (which separates the ground-state manifold to higher-energy states), as excitations across spectral gap may not lead to the fluctuations of the Hall conductance or contribute to the longitudinal conductance. Although the two gaps likely disappear simultaneously when disorder is large enough to destroy the quantum Hall state. Therefore we expect that P_{ext} rises sharply (probably abruptly) at the mobility gap in the thermodynamic limit, a signature imprinted in finite systems as well. Here, we find the sharpest jump of P_{ext} between one group and its lower neighboring group, and define the energy of the higher group as the mobility edge. We measure the mobility gap $E_m(N_e)$ from the ground-state energy to the mobility edge for the system of N_e electrons. Since the states in each group are degenerate in the thermodynamic limit, we use the average energy in each group to calculate $E_m(N_e)$ to reduce finite-size fluctuations. We then extrapolate E_m to the thermodynamic limit from $N_e=4$–8 electrons. We plot the resulting E_m as a function of W for various β in Fig. 7(a). The plot clearly demonstrates that finite layer thickness reduces the mobility gap as expected. In order to show the overall trend in the disorder dependence of the gap, particularly for weak disorder for various 2D layer thicknesses, we include the gaps for pure systems on y axes (for $W=0$ and $1/\mu=0$). The calculations of the pure gaps, which differ from the Chern number calculations in disordered systems,

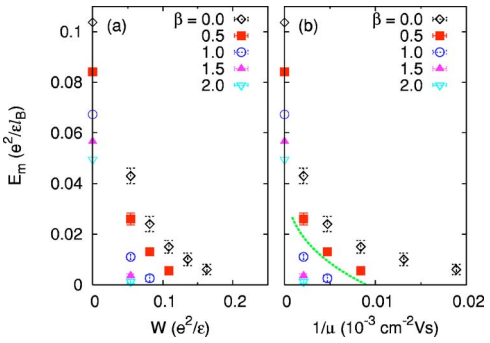

FIG. 7. (Color online) (a) Mobility gap E_m as a function of W for various layer thickness β. E_m is extrapolated from systems of $N_e=4$–8 electrons to the limit $1/N_e \to 0$. (b) Dependence of E_m on inverse mobility $1/\mu^0$ for various β. The dashed line is converted from a fit to experimental data (taken from Ref. 4). Here, we use an empirical mobility-density relation as well as a mobility-disorder relation in the Born approximation $\mu^0 = e\hbar^3/(m^{*2}W^2)$. The data points on the y axes (for $W=0$ and $1/\mu=0$) are the gaps for pure systems, whose calculations are illustrated in detail in Appendix B.

are illustrated in detail in Appendix B. Comparing Fig. 7(a) with Fig. 4(b), we find that the mobility gap and the spectral gap differ significantly for small disorder and small layer thickness, although they both decrease with increasing disorder, as well as with increasing layer thickness. The two gaps appear to disappear at roughly the same disorder strength.

In experiments, an energy gap Δ in the excitation spectrum of the correlated many-body ground state can be extracted from the temperature dependence of the magnetoresistivity, $\rho_{xx} \propto \exp(-\Delta/2k_BT)$, where k_B is the Boltzmann's constant and $\Delta/2$ is often referred as the activation energy.[3–5] This activation energy is related to the mobility gap we calculated, which separates the ground state from its delocalized quasiparticle excitations. Boebinger *et al.*[4] systematically studied the activation energy for $\nu=1/3, 2/3, 4/3$, and $5/3$ and its dependence on sample mobility μ (an indication of disorder) in a series of GaAs-$Al_xGa_{1-x}As$ samples. For a class of high-mobility (at that time—with mobility up to 10^6 cm^2/V s) samples, they found that $\Delta \simeq 0.049e^2/\epsilon l - 6$ K, consistent with a simple phenomenological model[3] that assumes a disorder-broadened excitation energy level with half width $\Gamma=6$ K. Willett *et al.* studied a then ultrahigh-mobility sample and compared the activation energy to theoretical results incorporating finite layer thickness[11] and Landau level mixing.[10,12] While the agreement between experimental results and theoretical caculations (in the absence of disorder) is satisfactory for magnetic field stronger than 10 T, they diverge significantly at smaller magnetic field, presumably due to disorder. Simple theories[13,14] with *ad hoc* treatment of disorder fail to account for all the discrepancies.

With our numerical calculations which treat disorder and layer thickness on an equal footing, we can now attempt to compare our results to experimental ones quantitatively. In experiments, the mobility μ dependence of Δ can then be extracted from the known dependence of μ on the electron density n of these samples, since n determines the magnetic field B (or l_B) at the 1/3 family of fillings. For semiquantitative comparison, we use a typical dependence, $\mu=\mu_0(n/n_0)^{1.5}$, where $\mu_0=600\,000$ cm^2/V s and $n_0=1.5\times10^{11}$ cm^{-2}, as extracted from Fig. 1 of Ref. 4. For comparison, we assume that in our simple disordered model both the (zero field) mobility and the (high field) mobility gap are dominated by short-range scatterers (appropriate for these then high-mobility samples). In the Born approximation (as derived in Appendix C), we have

$$\mu^0 = e\hbar^3/(m^{*2}W^2). \tag{18}$$

Figure 7(b) compares this empirical formula of $\Delta(\mu^0)$ with the mobility gap we obtained in our calculation for various β. We find that the experimental data fall nicely into the range of $0.5<\beta<1$. This is fully expected in typical experiments: the variational parameter b^{-1} for a typical GaAs-AlGaAs sample with an electron density of $N_0=10^{11}$ cm^{-2} is close to the magnetic length l_B,[11] which scales with $B^{-1/2}$ (e.g., $l_B=57$ Å for $B=20$ T). In particular, Willett *et al.* obtained $b^{-1}=39\pm1$ Å for their sample, giving $\beta=(bl_B)^{-1} \approx 0.68$ at $B=20$ T. We do not include, however, the effects of Landau level mixing, which leads only to a small reduction of the mobility gap for clean samples.[5,10]

IV. EFFECTS OF CORRELATED POTENTIAL

In this section, we briefly discuss the effects of impurity potential with finite correlation length for $\nu=1/3$. The correlated potential is, in particular, relevant to ultrahigh-mobility 2DEG, such as GaAs based systems in which impurities are introduced remotely above the 2DEG. The mobility of these systems is generally believed to be limited by remote impurity scattering, rather than by short-range interface defects. To consider the correlated potential effects, we introduce the Gaussian correlated random potential

$$\langle U_{\mathbf{q}} U_{\mathbf{q}'} \rangle = \frac{W^2}{A} \delta_{\mathbf{q},-\mathbf{q}'} e^{-q^2\xi^2/2}, \tag{19}$$

as described in detail in Sec. II. Here, we restrict ourselves, for simplicity, to bare Coulomb interaction without considering finite layer thickness. We are mostly interested in the case of small correlation length $\xi \sim 1$, in units of l_B, where quantitative results can be reached.

The results we find, in particular for $\xi=1$, are qualitatively similar to those with Gaussian white-noise potential.[33] Figure 8(a) compares the mobility gap E_m as a function of W for Gaussian white-noise potential ($\xi=0$) and Gaussian correlated potential with $\xi=1$. The trend that increasing disorder strength destroys the mobility gap is generically the same for impurity potential with or without correlation. However, E_m survives larger W (by a factor of roughly 50%) for $\xi=1$ than for $\xi=0$. This is not surprising since impurity potential correlation enhances the electron mobility, in particular for low-electron densities. As shown in Appendix C, the mobility of the 2DEG, in the Born approximation, is enhanced by a factor of

$$\frac{\mu}{\mu^0} = \frac{e^{k_F^2\xi^2}}{I_0(k_F^2\xi^2) - L_0(k_F^2\xi^2)}, \tag{20}$$

where $I_0(x)$ is the zeroth-order modified Bessel function of the first kind and $L_0(x)$ the zeroth-order modified Struve

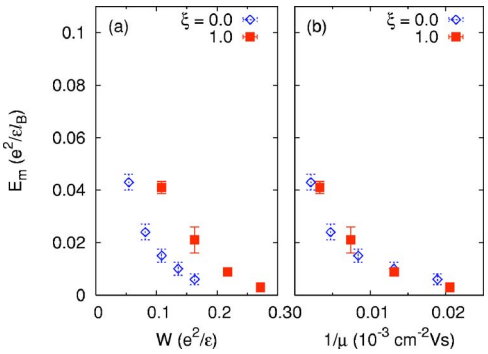

FIG. 8. (Color online) (a) Mobility gap E_m as a function of W for Gaussian correlated potential with $\xi=1.0$, in units of l_B, compared with Gaussian white-noise potential ($\xi=0$). (b) Dependence of E_m on inverse mobility $1/\mu$ for $\xi=1.0$ and 0.0.

function. Here, $k_F=\sqrt{4\pi n}=\sqrt{2\nu}/l_B$ is the Fermi vector of the polarized 2DEG. For $\xi=1$, the factor is $\mu/\mu^0=2.556$. In the long-range limit, one obtains

$$\frac{\mu}{\mu^0} \approx \sqrt{8\pi}(k_F\xi)^3. \tag{21}$$

Figure 8(b) shows the mobility gap E_m as a function of $1/\mu$ for impurity potentials with and without correlation, as we have done here and in an earlier paper.[33] Interestingly, E_m for $\xi=1$ scales back and lies roughly on top of the data for $\xi=0$. This suggests that as long as ξ is not too large, the effect of the range of potential can be lumped into that of sample mobility; this makes comparisons between samples of different types, as well as between theory and experiment, more meaningful, because the mobility is the directly measured character of a sample, while the details of disorder potential in general vary from sample to sample.

We do not have, however, quantitative conclusion for vary large ξ, which is believed to be responsible for those ultrahigh-mobility samples. Our finite-size calculations prevent us from considering large ξ close to or even larger than the system size, at which stage the system properties saturate. We would also need to calculate Chern numbers for a lot more eigenstates to obtain the mobility gap for the smooth potential, which is beyond our current computing capabilities. Nonetheless, it is expected that for those ultrahigh-mobility samples, disorder plays a less important role, and thus the mobility gap depends less on the mobility of a sample.[5]

V. CONCLUSIONS AND DISCUSSIONS

Semiconductor heterojunctions with modulation doping is the *de facto* fabrication technique for high-mobility quasi-two-dimensional samples commonly used for the study of the fractional quantum Hall effects. The range and strength of the impurity potential and the finite layer thickness of the systems can significantly affect the transport properties of the system, such as the activation gap of the fractional quantum Hall liquids. In this paper, we have studied these issues using a microscopic disordered model of the fractional quantum Hall liquids in a toroidal geometry. With the help of the Chern number calculation, which is capable of directly probing the localization properties of many-body states, we have determined the mobility edge of the Hall liquids based on the fluctuations of the Hall conductivity and studied the dependence of mobility gap on disorder strength, layer thickness, and potential correlation.

Finite 2D layer thickness has significant effects on the properties of the 2DEG in experimental samples. The spread of the electron wave function in the perpendicular direction softens the Coulomb interaction between electrons, reflected both in the density of states and in the ground-state energy of the system. Consequently, the spectral gap, which separates ground-state manifold from excited states, decreases with increasing layer thickness, as well as with increasing disorder strength. The mobility gap, associated with the fluctuation of topological Chern numbers—signaling delocalized excitations, also decreases with increasing layer thickness and disorder. However, the two gaps are different by definition and, indeed, distinguishable in numerical calculations, in particular for small layer thickness and weak disorder. Putting reasonable experimental parameters, we found our results of the mobility gap are in excellent agreement with the activation gap measured by experiments, suggesting that the mobility gap is responsible for the activated behavior in longitudinal resistivity. Disorder and 2D layer thickness are the two dominant factors affecting the value of the gap.

We also investigate the effect of the correlated disordered potential on the mobility gap. For small correlation length, we found an enhancement in the mobility gap compared to the case of uncorrelated potential for the same disorder strength. Such enhancement is consistent with the enhancement in mobility of the 2DEG in the presence of the correlated potential. As long as the correlation length is small, the effect of the correlated potential can be attributed to that of the sample mobility, which demonstrates it meaningful to compare the gap as a function of mobility among samples of different types and between theory and experiment.

In this paper, we model the electron wave function in the perpendicular direction by the variational Fang-Howard wave function. This is appropriate for modulation-doped GaAs-$Al_xGa_{1-x}As$ heterojunctions, in which the Fang-Howard function is a very good approximation to the numerical self-consistent ground-state wave function.[39] For realistic values of layer thickness, the qualitative nature of the ground states and the low-energy excitations of the quasi-two-dimensional systems remains unchanged, in particular in the incompressible phases.

Meanwhile, Shayegan *et al.*[40] studied the fractional quantum Hall effects in thick parabolic quantum wells. Due to the selective doping of Al and screening, electrons experience a flat potential and therefore the electron density are roughly uniform in the quantum well. This results in a significantly larger layer thickness, which increases with electron areal density. In such a system, Shayegan *et al.*[40] observed a dramatic decrease in the activation gap with increasing layer thickness and thus the collapse of the fractional quantum Hall effect. He *et al.*[41] studied the effects of layer thickness using a phenomenological model potential (neglecting the accompanying effects of Landau level mixing) and obtained

qualitatively consistent results to the experimental measurements. Although we have not repeated our calculations with a different wave function more suitable for a parabolic quantum well, we expect a similar trend of decreasing mobility gap with increasing layer thickness. We would like to point out that Fig. 7 clearly demonstrates that increasing layer thickness can trigger a transition from a $\nu=1/3$ fractional quantum Hall liquid to an insulator for fixed disorder strength. The transition becomes easier to occur in the presence of larger disorder.

ACKNOWLEDGMENTS

This work was supported by the Schwerpunktprogramme "Quanten-Hall-Systeme" der DFG (X.W.), ACS-PRF 41752-AC10 (D.N.S.), US DOE under Contract DE-FG03-02ER-45981 (E.H.R.), NSF Grant Nos. DMR-0307170 (D.N.S.), DMR-0225698 (K.Y.), and NSF under MRSEC Grant No. DMR-0213706 at the Princeton Center for Complex Materials (R.N.B. and F.D.M.H.). F.D.M.H. wishes to thank the KITP for support (NSF Grant No. PHY99-07949) during his visit.

APPENDIX A: GROUND-STATE ENERGY OF A TWO-DIMENSIONAL SQUARE WIGNER LATTICE WITH FINITE LAYER THICKNESS

We calculate the ground-state energy of finite-size systems with periodic boundary conditions. To compare our results with earlier works,[35,36] we must add, to our numerical ground-state energy, a single-electron contribution from the interaction of an electron and its images due to periodic boundary conditions (see also Appendix B). In an ideal two-dimensional square system of linear size $L=\sqrt{2\pi N_s}l_B$, this is simply the Madelung energy of a square lattice with lattice constant L and, for each electron, is[42,43]

$$\epsilon_M = -\frac{e^2}{L}\left(2-\sum_{l_1,l_2}{}'\phi_{-1/2}[\pi(l_1^2+l_2^2)]\right) = -\frac{3.9e^2}{2L} \quad \text{(A1)}$$

calculated first in the context of the Coulomb energy of the two-dimensional classical Wigner crystal.[44] The summation is performed over lattice sites $\mathbf{l}=l_1\mathbf{a}_1+l_2\mathbf{a}_2$ for the primitive lattice vectors $\mathbf{a}_1$ and $\mathbf{a}_2$ except $\mathbf{l}=0$ and the $\phi_n(x)$ are the Misra functions

$$\phi_n(x) = \int_1^\infty dt\, t^n e^{-xt}. \quad \text{(A2)}$$

The factor of $1/2$ in Eq. (A1) comes from the double counting of the electron-electron interaction.

In the presence of finite layer thickness, the Coulomb energy of the quasi-two-dimensional classical Wigner crystal is also known for generic lattices.[45] The wave function $\phi(z)$ in the perpendicular direction enters through the following function:

$$f(y,b) = \int_0^\infty dz \int_0^\infty dz'\, \phi^2(z)\phi^2(z')e^{-y|z-z'|} \quad \text{(A3)}$$

and for the Fang-Howard wave function

$$\phi(z) = (b^3/2)^{1/2} z e^{-bz/2}, \quad \text{(A4)}$$

one can obtain $f(y,b)=\tilde{f}(b^2/4y)$, where

$$\tilde{f}(t) = \frac{3t}{4} - \frac{t^2}{2} + \sqrt{t}e^t\left(\frac{3}{8}-\frac{t}{2}+\frac{t^2}{2}\right)\Gamma\left(\frac{1}{2},t\right). \quad \text{(A5)}$$

Here, the incomplete gamma function $\Gamma(a,x)$ is given by

$$\Gamma(a,x) \equiv \int_x^\infty dt\, t^{a-1}e^{-t} = x^a \phi_{a-1}(x). \quad \text{(A6)}$$

For $a=1/2$, the incomplete gamma function is also related to the complementary error function

$$\mathrm{erfc}(z) = \frac{2}{\sqrt{\pi}}\int_z^\infty dt\, e^{-t^2} = \frac{\Gamma\left(\frac{1}{2},z^2\right)}{\sqrt{\pi}}, \quad \text{(A7)}$$

for $z>0$.

With the help of an integral transform, one can replace the slowly converging sum of Coulomb energy into two rapidly converging sums: one for the short-range part and the other the long-range part, in the same spirit as in the original Ewald method.[44] In the following, the parameter that separates the two sums is denoted as y_0, chosen to be π/L^2 in our calculation. For convenience, one introduces the Jacobi θ function

$$\theta(z,X) = \sum_{m=-\infty}^{\infty} e^{2\pi m z}e^{-\pi m^2 X}, \quad \text{(A8)}$$

which converges fast for not too small X. Here, we only review the results for a square lattice with lattice constant L for simplicity. To be specific, they are the $q\to 0$ limit of Eqs. (16)–(21) in Ref. 45 for the square lattice. The Coulomb energy per electron for the square lattice can be written as

$$N_e^{-1}E_{ee} = N_e^{-1}E_{ee}^{>} + N_e^{-1}E_{ee}^{<}, \quad \text{(A9)}$$

where

$$\frac{E_{ee}^{>}}{N_e} = \frac{e^2}{2\sqrt{\pi}}\int_{y_0}^\infty dy\, y^{-1/2} f(y,b)\left[\theta^2\left(0;\frac{L^2 y}{\pi}\right)-1\right] \quad \text{(A10)}$$

and

$$\begin{aligned}\frac{E_{ee}^{<}}{N_e} = {} & \frac{\sqrt{\pi}e^2}{2L^2}\int_0^{y_0} dy\, y^{-3/2} f(y,b)\left[\theta^2\left(0;\frac{\pi}{L^2 y}\right)-1\right] \\ & - \frac{\sqrt{\pi}e^2}{2L^2}\int_{y_0}^\infty dy\, y^{-3/2} f(y,b) - \frac{e^2}{2\sqrt{\pi}}\int_0^{y_0} dy\, y^{-1/2} f(y,b) \\ & + N_e^{-1}E_{ee}^{hom}(q)|_{q=0}, \end{aligned} \quad \text{(A11)}$$

where $E_{ee}^{hom}(q)$ is the Coulomb energy corresponding to a homogeneous distribution,

$$N_e^{-1}E_{ee}^{hom}(q) = \frac{\sqrt{\pi}e^2}{2L^2}\int_0^{y_0} dy\, y^{-3/2} f(y,b) e^{-q^2/4y}$$
$$= \frac{\pi e^2}{L^2}\left(\left.\frac{1}{q}\right|_{q=0} - \frac{15}{8b}\right). \quad \text{(A12)}$$

Here the singular $1/q$ term has its origin in the lack of charge neutrality considered here. In fact, only nonsingular terms survive in the total Coulomb energy once neutralizing background charge (e.g., located uniformly at $z=-b_d$) is present. The second term, as well as additional nonsingular terms introduced by the interactions between electrons and the background charge, depends only on "external" parameters, such as layer thickness b and location of the background charge b_d. We neglected these terms since they have no effects on the results of the finite-size scaling in the $1/N_e \to 0$ limit.

APPENDIX B: CALCULATIONS OF THE GAPS IN PURE SYSTEMS WITH LAYER THICKNESS

In order to show the overall trend in the disorder dependence of the gap, particularly for weak disorder for various 2D layer thicknesses, we presented the pure gaps ($1/\mu=0$, $W=0$) in Fig. 7 for $\nu=1/3$. In this appendix we give the main details. These types of calculations in PBC geometry have so far been largely avoided for fear of strong finite-size effects. These result from the interaction of the quasiparticles with their images. Indeed such effects remain substantial (as large as 30% in some cases) for even the largest sizes in exact diagonalization studies. In order to remove these we follow the practice of not neutralizing the quasiparticle (qp) and quasihole (qh) excitations.[8] This gives a positive contribution of

$$\frac{e^{*2}}{2\epsilon A}\int d^2\vec{r} V(r), \quad \text{(B1)}$$

where $e^*=e/3$ is the charge of the quasiparticle excitation, A is the area of the system, and

$$V(r) = \int d^2\vec{q}\frac{2\pi}{q}\exp\{i\vec{q}\cdot\vec{r}\}, \quad \text{(B2)}$$

where $\vec{q}=n_1\vec{G}_1+n_2\vec{G}_2$ is the wave vector appropriate for the PBC unit cell, $\vec{G}$'s are the corresponding reciprocal-lattice vectors, and n's are integers. We next subtract the repulsive interaction energy of a single quasiparticle with its images:

$$\frac{e^{*2}}{2\epsilon}\sum_{\ell_1,\ell_2=-\infty}^{\infty}\frac{1}{|\vec{X}(\vec{\ell})|}, \quad \text{(B3)}$$

where $\vec{X}(\vec{\ell})=\ell_1\vec{L}_1+\ell_2\vec{L}_2$, ℓ's are integers and $\vec{L}$'s are the direct lattice vectors. These two terms together add to

$$\delta E = (e^*/e)^2|S| = |S|/9, \quad \text{(B4)}$$

where S is the classical ground-state energy per electron (Madelung energy) of a Wigner crystal of electrons.[44,46] Note that we are treating the quasiparticles as point objects. This approximation only introduces another finite-size effect since the size of the unit cell is several magnetic lengths whereas the substantial density variation of the quasiparticle excitations occurs over a magnetic length.

TABLE I. Gaps in pure FQHE systems at $\nu=1/3$ for various 2D layer thickness.

β	0.0	0.5	1.0	1.5	2.0
Δ	0.1037	0.08410	0.06729	0.05656	0.04940

Starting from the usual expression of the gap in terms of the ground-state energies:

$$\Delta = E(\nu=1/3+qp) + E(\nu=1/3+qh) - 2E(\nu=1/3). \quad \text{(B5)}$$

With the above subtractions we obtain

$$\Delta^* = E^*(\nu=1/3+qp) + E^*(\nu=1/3+qh) - 2E^*(\nu=1/3) + \delta E_{qp} + \delta E_{qh}, \quad \text{(B6)}$$

where E^* is the finite part of the energy without the Madelung term ($E^*=E-NS$) (note that S is negative). This contribution taken together for the three ground-state energies in Δ^* is a finite-size effect as are both δE energies so they will disappear in the thermodynamic limit ($\Delta^*_\infty=\Delta_\infty$). Therefore we need not correct any of these energies for finite layer thickness. We then extrapolate Δ^* to the thermodynamic limit from its $1/N$ dependence. We used the hexagonal unit cell for this part as it has the highest degree of symmetry. Table I gives the numerical values of the Δ_∞ that we have obtained from $N=7$–10 size systems. In the same table we give the corresponding results for the finite layer systems. We have shown all these on the y axis of Fig. 7 (for $1/\mu=0$ and $W=0$).

APPENDIX C: MOBILITY OF TWO-DIMENSIONAL NONINTERACTING ELECTRONS IN RANDOM POTENTIAL

In this appendix, we review the results of the mobility of a two-dimensional noninteracting electron system with a random potential in standard perturbation theory[47] and apply them to our model system.

Consider spinless electrons in a quenched random potential $U(r)$ with Gaussian correlation

$$\langle U(\mathbf{r})U(\mathbf{r}')\rangle = \frac{W^2}{2\pi\xi^2}e^{-|\mathbf{r}-\mathbf{r}'|^2/2\xi^2} \equiv W(|\mathbf{r}-\mathbf{r}'|), \quad \text{(C1)}$$

where ξ is the characteristic correlation length. Note that in the limit of $\xi\to 0$, we recover

$$\langle U(\mathbf{r})U(\mathbf{r}')\rangle = W^2\delta(\mathbf{r}-\mathbf{r}') \quad \text{(C2)}$$

for a Gaussian white-noise potential. The total scattering rate in the Born approximation is[47]

$$\frac{1}{\tau_{tr}} = \frac{2\pi\rho}{\hbar}\int_0^{2\pi}\frac{d\phi}{2\pi}\tilde{W}\left(2k_F\sin\frac{\phi}{2}\right)(1-\cos\phi)$$
$$= \frac{4\pi^2\rho}{\hbar}\int_0^{\infty} dr\, r[J_0^2(k_F r) - J_1^2(k_F r)]W(r), \qquad \text{(C3)}$$

where $\rho = m^*/(2\pi\hbar^2)$ is the density of states of free electrons and $k_F = \sqrt{4\pi n} = \sqrt{2\nu}/l_B$ is the Fermi vector. $\tilde{W}(k)$ is the Fourier transformation of $W(r)$

$$\tilde{W}(k) = \int d^2 r W(r)\exp(-i\mathbf{k}\cdot\mathbf{r}). \qquad \text{(C4)}$$

For the Gaussian white-noise potential, $\tilde{W}(k) = W^2$, thus

$$\frac{1}{\tau_{tr}} = \frac{m^* W^2}{\hbar^3}. \qquad \text{(C5)}$$

The mobility of the system with the short-range potential is therefore

$$\mu^0 = \frac{e\tau_{tr}}{m^*} = \frac{e\hbar^3}{m^{*2}W^2}. \qquad \text{(C6)}$$

With simple algebras, we can rewrite the mobility μ in terms of the cyclotron energy $\hbar\omega_c$, the Coulomb energy $e^2/\epsilon l_B$, and the magnetic length l_B as

$$\mu^0 = \frac{e}{\hbar}l_B^2\left[\frac{\hbar\omega_c}{e^2/\epsilon l_B}\right]^2\frac{1}{\bar{W}^2}, \qquad \text{(C7)}$$

where $\bar{W} = \epsilon W/e^2$ is the dimensionless disorder strength.

For a long-range potential, $k_F\xi \gg 1$, one finds[47]

$$\frac{1}{\tau_{tr}} = -\frac{m}{(\hbar k_F)^3}\int_0^{\infty} dr\frac{W'(r)}{r}. \qquad \text{(C8)}$$

In particular, for the Gaussian correlated potential,

$$\tilde{W}(k) = W^2 e^{-k^2\xi^2/2}, \qquad \text{(C9)}$$

we can integrate Eq. (C3) and obtain

$$\frac{1}{\tau_{tr}} = \frac{m^* W^2}{\hbar^3}e^{-k_F^2\xi^2}\left[I_0(k_F^2\xi^2) - L_0(k_F^2\xi^2)\right], \qquad \text{(C10)}$$

where $I_0(x)$ is the zeroth-order modified Bessel function of the first kind and $L_0(x)$ the zeroth-order modified Struve function.[48] The mobility of the system with the Gaussian correlated potential is therefore

$$\mu = \mu^0\frac{e^{k_F^2\xi^2}}{I_0(k_F^2\xi^2) - L_0(k_F^2\xi^2)}. \qquad \text{(C11)}$$

In the long-range limit, we obtain

$$\frac{\mu}{\mu^0} \simeq \sqrt{8\pi}(k_F\xi)^3. \qquad \text{(C12)}$$

[1] K. v. Klitzing, G. Dorda, and M. Pepper, Phys. Rev. Lett. **45**, 494 (1980).
[2] D. C. Tsui, H. L. Störmer, and A. C. Gossard, Phys. Rev. Lett. **48**, 1559 (1982).
[3] A. M. Chang, M. A. Paalanen, D. C. Tsui, H. L. Stormer, and J. C. M. Hwang, Phys. Rev. B **28**, 6133 (1983).
[4] G. S. Boebinger, H. L. Stormer, D. C. Tsui, A. M. Chang, J. C. M. Hwang, A. Y. Cho, C. W. Tu, and G. Weimann, Phys. Rev. B **36**, 7919 (1987).
[5] R. L. Willett, H. L. Stormer, D. C. Tsui, A. C. Gossard, and J. H. English, Phys. Rev. B **37**, 8476 (1988).
[6] See, for example, R. E. Prange and S. M. Girvin, *The Quantum Hall Effect*, 2nd ed. (Springer-Verlag, Berlin, 1990).
[7] R. B. Laughlin, Phys. Rev. Lett. **50**, 1395 (1983).
[8] F. D. M. Haldane and E. H. Rezayi, Phys. Rev. Lett. **54**, 237 (1985).
[9] S. M. Girvin, A. H. MacDonald, and P. M. Platzman, Phys. Rev. Lett. **54**, 581 (1985).
[10] D. Yoshioka, J. Phys. Soc. Jpn. **55**, 885 (1986).
[11] F. C. Zhang and S. Das Sarma, Phys. Rev. B **33**, 2903 (1986).
[12] D. Yoshioka, J. Phys. Soc. Jpn. **53**, 3740 (1984).
[13] A. H. MacDonald, K. L. Liu, S. M. Girvin, and P. M. Platzman, Phys. Rev. B **33**, 4014 (1985).
[14] A. Gold, Europhys. Lett. **1**, 241 (1986).
[15] A. Gold, Phys. Rev. B **36**, 3268 (1987).
[16] D. J. Thouless, M. Kohmoto, M. P. Nightingale, and M. den Nijs, Phys. Rev. Lett. **49**, 405 (1982).
[17] Q. Niu, D. J. Thouless, and Y. S. Wu, Phys. Rev. B **31**, 3372 (1985).
[18] D. P. Arovas, R. N. Bhatt, F. D. M. Haldane, P. B. Littlewood, and R. Rammal, Phys. Rev. Lett. **60**, 619 (1988).
[19] Y. Huo and R. N. Bhatt, Phys. Rev. Lett. **68**, 1375 (1992).
[20] D. N. Sheng and Z. Y. Weng, Phys. Rev. Lett. **75**, 2388 (1995).
[21] D. N. Sheng and Z. Y. Weng, Phys. Rev. B **54**, R11070 (1996).
[22] K. Yang and R. N. Bhatt, Phys. Rev. B **55**, R1922 (1997).
[23] R. N. Bhatt and X. Wan, Pramana, J. Phys. **58**, 271 (2002).
[24] J. E. Avron, R. Seiler, and B. Simon, Phys. Rev. Lett. **51**, 51 (1983).
[25] B. Simon, Phys. Rev. Lett. **51**, 2167 (1983).
[26] J. E. Avron, D. Osadchy, and R. Seiler, Phys. Today **56** (8), 38 (2003).
[27] J. E. Avron and R. Seiler, Phys. Rev. Lett. **54**, 259 (1985).
[28] R. Tao and Y. S. Wu, Phys. Rev. B **30**, 1097 (1984).
[29] F. C. Zhang, V. Z. Vulovic, Y. Guo, and S. Das Sarma, Phys. Rev. B **32** 6920 (1985).
[30] R. Tao and F. D. M. Haldane, Phys. Rev. B **33**, 3844 (1986).
[31] X.-G. Wen and Q. Niu, Phys. Rev. B **41**, 9377 (1990).
[32] X.-G. Wen, *Quantum Field Theory of Many-Body Systems* (Oxford University Press, New York, 2004).
[33] D. N. Sheng, X. Wan, E. H. Rezayi, K. Yang, R. N. Bhatt, and F. D. M. Haldane, Phys. Rev. Lett. **90** 256802 (2003).
[34] D. J. Thouless, Phys. Rev. B **40**, 12034 (1989).
[35] A. H. MacDonald and G. C. Aers, Phys. Rev. B **29**, 5976 (1984).
[36] T. Chakraborty, Phys. Rev. B **34**, 2926 (1986).

[37] D. Pfannkuche and A. H. MacDonald, Phys. Rev. B **56**, R7100 (1997).
[38] N. E. Bonesteel, Phys. Rev. A **62**, 062310 (2000), and the references therein.
[39] F. Stern and S. Das Sarma, Phys. Rev. B **30**, 840 (1984).
[40] M. Shayegan, J. Jo, Y. W. Suen, M. Santos, and V. J. Goldman, Phys. Rev. Lett. **65**, 2916 (1990).
[41] S. He, F. C. Zhang, X. C. Xie, and S. Das Sarma, Phys. Rev. B **42**, R11376 (1990).
[42] D. Yoshioka, B. I. Halperin, and P. A. Lee, Phys. Rev. Lett. **50**, 1219 (1983).
[43] W. P. Su, Phys. Rev. B **30**, 1069 (1984).
[44] L. Bonsall and A. A. Maradudin, Phys. Rev. B **15**, 1959 (1977).
[45] N. M. Fujiki and D. J. W. Geldart, Phys. Rev. B **46**, 9634 (1992). Note that the definition of the layer thickness parameter b is different from the one used in this work.
[46] D. Yoshioka, Phys. Rev. B **29**, 6833 (1984).
[47] See, for example, A. D. Mirlin, E. Altshuler, and P. Wölfle, Ann. Phys. (Leipzig) **5**, 281 (1996).
[48] *Handbook of Mathematical Functions with Formulas, Graphs, and Mathematical Tables*, NBS Applied Mathematics Series No. 55, edited by M. Abramowitz and C. A. Stegun (National Bureau of Standards, Washington, DC, 1964).